Dynamic Structure of Poly(*p*-phenyleneterephthalamide)‡

R. J. Schadt,† K. H. Gardner, V. Gabara, S. R. Allen, D. B. Chase, and A. D. English*

DuPont Central Research and Development and DuPont Fibers, Experimental Station, Wilmington, Deleware 19880–0356

Received April 19, 1993; Revised Manuscript Received August 5, 1993•

ABSTRACT: The *dynamic structure* of poly(*p*-phenyleneterephthalamide) (PPTA) is examined for the *p*-phenylenediamine ring sites. This information is melded with other ^2H NMR results concerning the segmental dynamic structure of the terephthalamide rings and the amide sites as well as morphological studies to develop a description of the dynamic structure on the length scale of 1–100 Å. The PPTA dynamic structure is characterized by the presence of two populations: one of which is associated with crystal surfaces (alternatively crystal packing defect planes) and accounts for approximately 30% of all the diamine rings, and the other population is associated with the crystallite interior (more perfectly formed planes). Each of these populations is dynamically heterogeneous, reflecting the packing imperfections of each population.

Introduction

In previous papers, the segmental dynamics of the terephthalamide rings[1–3] and amide sites[4,5] of poly(*p*-phenyleneterephthalamide) (PPTA) have been characterized over a wide temperature range with ^2H NMR methods. These studies characterized the *dynamic structure*[6] of PPTA, for both crystal modifications,[7,8] in terms of sites associated either with the surfaces of crystallites (or alternatively crystal packing defect planes) or the interior of the crystallites. The dynamic structure of the terephthalamide rings[1–3] was modeled as a temperature-dependent population of mobile rings which reflected the heterogeneity of the dynamic structure for both the crystallite surface and interior. ^2H NMR line shapes for the amide sites[4] could be decomposed into a major component (~75%) associated with relatively rigid amide sites and a minor component (~25%) associated with a fraction of mobile amide bonds which execute large-angle jumps. This behavior of the amide sites was determined to be essentially temperature-independent over a range of −184 to +228 °C. In combination with structural features observed by X-ray diffraction and transmission electron microscopy,[5] this discrimination of amide mobility is identified as deriving from incompletely hydrogen-bonded sites located at the crystallite surface or defect regions of the highly crystalline[9] polymer.

Further details of the dynamic structure of PPTA are available from the results of the ^2H NMR investigation of diamine ring deuterated PPTA presented here. To interpret the ^2H NMR spin–lattice relaxation and the quadrupole echo delay time dependence of the fully-relaxed spectra, a model is developed which semiquantitatively accounts for both the molecular motions of the diamine rings and the previously observed dynamics of the terephthalamide rings[1–3] within PPTA. As a result, this study supports the conclusion not only that the dynamic structure of PPTA is heterogeneous in the sense that sites located at crystallite surfaces (defect regions) exhibit enhanced mobility relative to those located at the crystallite interior (more perfectly formed planes) but also that both populations exhibit a distribution of mobilities and hence are heterogeneous.

* To whom correspondence should be addressed.
† Current address: Polymer Division, Building 224, Room A209, NIST, Gaithersburg, MD 20899.
‡ Contribution No. 6432.
• Abstract published in *Advance ACS Abstracts*, October 15, 1993.

Experimental and Calculational Procedures

Material Synthesis. Diamine ring perdeuterated PPTA (polymorph I′) with M_n ~25 000, inherent viscosity of 7.5 dL/g in 98% H_2SO_4, was prepared by reaction of 99+% isotopic purity *p*-phenylenediamine-d_8 (PPD-d_8) (MSD Isotopes, Division of Merck Frosst Canada, Inc., Montreal, Canada) with terephthaloyl chloride (TCl) in an 8% solution of $CaCl_2$ in *N*-methylpyrrolidone.[10] In a three-necked resin kettle equipped with a stirrer and dry nitrogen purge, PPD-d_8 (5.7 g) was dissolved in 180 g of the solvent system and the temperature was lowered to 10 °C by external cooling with ice. TCl (10.0 g) was added into the mixture and the agitator speed was increased to maintain mixing as the viscosity of the reaction mixture increased. The material solidified into a gel and then broke into fine particles. After 15 min the reaction was terminated by addition of water. The polymer was washed with water to remove solvent and salt, and then the polymer was dried.

To confirm the isotopic composition of the polymer, samples were packed into 5-mm-diameter glass tubes, dried under vacuum at 200 °C for 24 h followed by an additional 4 days at 100 °C, and examined by FT-Raman spectroscopy.[11] Using 300 mW of 1.064-μm radiation from a LDI-3000 diode pumped Nd/YAG laser, scattered radiation was analyzed by a Nicolet 800 series interferometer equipped with an FT-Raman accessory. A Ge detector (North Coast, NEP = 10^{-15} W/Hz$^{1/2}$) was used and Rayleigh line filtering was accomplished with two Kaiser Optical Supernotch holographic filters. Two thousand scans, at 2-cm^{-1} nominal resolution, were averaged, resulting in a total measurement time of 1 h. The intensities were corrected for the instrument response function using a calibrated tungsten source. Spectra obtained after extensive irradiation established that no detectable polymer degradation occurred during collection of the FT-Raman spectra. A slight fluorescent background was observed, but it did not obscure the Raman features of interest. The FT-Raman spectrum revealed residual deuterated amide groups (N–D; 2400–2500-cm^{-1} region) which were subsequently exchanged to N–H by preparing a 1% solution of the polymer in 98% H_2SO_4, precipitating in a water/ice mixture, washing with water to remove sulfuric acid, and drying at 140 °C. A lower inherent viscosity (6 dL/g) was found after exchange. Using an identical drying procedure, as described above, FT-Raman spectroscopy confirmed that only the diamine rings were labeled with deuterium.

NMR Measurements. Fully- and partially-relaxed ^2H NMR spectra and associated spin–lattice relaxation data were obtained over a temperature range of −80 to +230 °C with a Bruker MSL 200 spectrometer operating at a resonance frequency of 30.72 MHz. The NMR probe was tuned following the multiple pulse tuning procedure of Gerstein[12] at all temperatures, using a sample of liquid acetone-d_6 at low temperatures and a sample of liquid D_2SO_4 at high temperatures, to minimize spectral distortion.[13–15] The temperature was controlled by a Bruker B-VT 1000 unit over a range of −80 to +230 °C which had been previously calibrated.[16]

0024-9297/93/2226-6509$04.00/0

Fully-relaxed spectra were acquired with a standard quadrupolar echo pulse sequence $[(\pi/2)_x - \tau_1 - (\pi/2)_{-y} - DO - (\pi/2)_{-x} - \tau_1 - (\pi/2)_{-y} - DO]$ where the data are acquired during the DO period and alternately added and subtracted. The $\pi/2$ radio frequency pulse was nominally 2.8 μs in length, τ_1 is the delay time which was set to 20, 40, 80, and 160 μs, and DO is the recycle delay time which was varied so that it was at least 5 times the spin–lattice relaxation time of the slowest relaxing component (T_{1long}) in the spectrum at a given temperature. The $\pi/2$ pulse width was sufficiently short to allow spectral acquisition with minimal spectral distortion.[17] Data (4096 points) were acquired at a rate of 2 MHz and then shifted to the top of the spin echo prior to Fourier transformation.

Spin–lattice relaxation times (T_1) were measured over a temperature range of −80 to +230 °C using a saturation recovery method. The pulse sequence was $[((\pi/2)_x - t)_9 - (\pi/2)_x - \tau_0 - (\pi/2)_x - \tau_1 - (\pi/2)_{-y} - DO - ((\pi/2)_{-x} - t)_9 - (\pi/2)_{-x} - \tau_0 - (\pi/2)_{-x} - \tau_1 - (\pi/2)_{-y} - DO]$, where t has a value of 3 ms, τ_0 is varied from 2.5 ms to 60 s, τ_1 has a value of 20 μs, and the data are acquired during the DO period and alternately added and subtracted. Spin–lattice relaxation of the selectively deuterated diamine rings was nonexponential and could be decomposed in the time domain into two components whose relaxation times differed by at least a factor of 21 over the temperature range −80 to +107 °C. Above 107 °C, T_1 discrimination was ineffective. Values of T_1, calculated from the evolution of the total magnetization as a function of τ_0 in the time domain, were determined by least squares fitting of the data to a sum of two exponential functions corresponding to a fast-relaxing component (T_{1short}) and a slow-relaxing component (T_{1long}). The same pulse sequence was used to obtain partially-relaxed spectra ($\tau_0 = 5 \times T_{1short}$). Partially-relaxed spectra were subtracted from corresponding fully-relaxed spectra to obtain spectra of those spins with the longest spin–lattice relaxation time.

NMR Line Shape Simulation. Using a simplified model for the dynamics of the diamine rings (see Results and Discussion), line shapes were calculated for discrete, equal population, two-site jumps (π-flips) about the 1,4-diamine ring axis using a previously described program[16] running on a Cray YMP or Silicon Graphics R-4D/280SX system. This program generates a zero-delay ($\tau_1 = 0$) line shape which is then corrected for echo distortions.[18] The correlation time τ_c in s/rad of the two-site jump is related to the residence time (τ') in s/cycle by $\tau_c = \tau'/(4\pi)$, and the correlation frequency (in Hz) is defined as $\nu_c = (2\pi\tau_c)^{-1}$. The calculated powder pattern is corrected for finite pulse length[17] and convoluted with Gaussian and Lorentzian broadenings, but no correction for molecular motion during the radio frequency pulses is used.[19] Typically, Gaussian broadening is determined from comparison of calculated line shapes to the low-temperature experimental spectra to account for residual dipolar interactions with neighboring ^{2}H and ^{1}H nuclei. Lorentzian broadening corresponds to the value used for processing of the experimental data (1 kHz full width half-maximum). Since the $\pi/2$ pulse length of 2.8 μs was previously determined to be lengthened by the nonpurely resistive load characteristics of the NMR probe,[16] all calculations used the previously utilized 3.2 μs pulse length.

In addition to two-site jump motion, rapid restricted angle fluctuations can be introduced into the calculation[16] by allowing each of the sites to undergo rapid librational motion characterized by an inhomogeneous librational amplitude distribution $P(\theta)$. For each orientation of the static magnetic field H_0, a series of 30–50 isochromats corresponding to 30–50 azimuthal librational angles (standard deviation $\Delta\theta$) is generated for each well of each site. The 30–50 isochromats are averaged with a population-weighted Gaussian distribution $P(\theta)$ to yield an isochromat which reflects the rapid librational motion within each well. The resulting two spin isochromats are then allowed to exchange with a residence time τ', and the line shape is corrected for the delay between quadrature pulses by using the correction factor $K(2\tau_1)$ from the exact theory.[18] This procedure is repeated for 1° steps in both polar and azimuthal angles of H_0 in the molecular frame to yield a powder pattern.

Distributions of correlation times are introduced by specifying a mean correlation time $\langle\tau_c\rangle$ (in Hz^{-1}) and standard deviation σ (in decades) for a log–Gaussian, population-weighted summation of a basis set of line shapes. Initial values for the mean correlation time and standard deviation of the correlation time distribution could be determined from a previous study of 1-D ^{2}H NMR line shapes for a π-flip model of motion.[20] More precise estimates of $\langle\tau_c\rangle$ and σ were determined from a semiquantitative fit of the line shapes which used a basis set ($\eta = 0$; $e^2qQ/h = 180$ kHz) consisting of a slow exchange, Pake-like line shape ($\tau_c > 10^{-2}$ s; Gaussian broadening of 3 kHz), intermediate exchange π-flip line shapes (10^{-2} s $\geq \tau_c \geq 10^{-7}$ s; five line shapes calculated per decade; Gaussian broadening of 1 kHz), and a fast exchange π-flip line shape ($\tau_c < 10^{-7}$ s; Gaussian broadening of 1 kHz) with a bimodal distribution of librational amplitudes $P(\Delta\theta)$. Distributions of jump angles ($P(\phi)$) and librational amplitudes ($P(\Delta\theta)$) were introduced by calculating the population-weighted summation of the line shapes according to the inhomogeneous distribution $P(\phi)$ or $P(\Delta\theta)$.

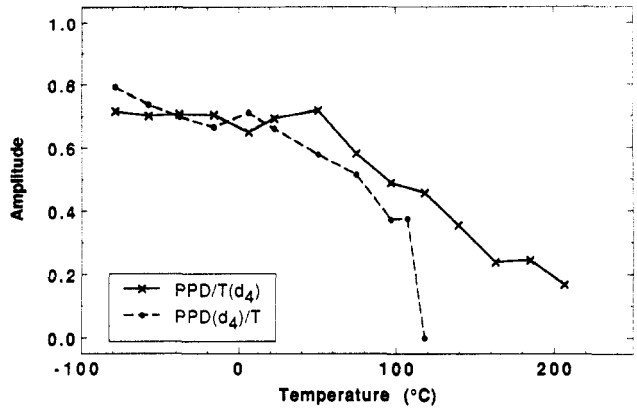

Figure 1. Spin–lattice magnetization amplitude (long T_1 component) vs temperature for both terephthalamide-d_4 and diamine-d_4 labeled poly(*p*-phenyleneterephthalamide).

Results and Discussion

Spin–Lattice Relaxation. In Figure 1, the spin–lattice magnetization amplitude associated with the long-T_1 component as a function of temperature is given for both terephthalamide-d_4 and diamine-d_4 PPTA. Spin–lattice relaxation of the selectively deuterated diamine rings was strongly nonexponential and could be decomposed in the time domain into two components, associated with long- and short-T_1 components, over a temperature range of −80 to +107 °C. Above 107 °C, T_1 discrimination was ineffective for the diamine ring deuterated PPTA (PPD-(d$_4$)/T). Similarly, the spin–lattice relaxation of the terephthalamide ring deuterated PPTA (PPD/T(d$_4$)) could be decomposed in the time domain into two components whose relaxation times differed by at least a factor of 30 over a temperature range of −80 to +207 °C, the discrimination becoming ineffective above 207 °C. The amplitude of the long-T_1 component in the low-temperature range is near 70–80% for both terephthalamide and diamine rings. The temperature dependence of the amplitude of the long-T_1 component is illustrated in Figure 1; this population (long-T_1 component) can be separated into two temperature regimes with a break near 50 °C for PPD(d$_4$)/T and a break near 70 °C for PPD/T(d$_4$). The separation of the spin–lattice relaxation components into two temperature regimes is consistent with discrimination of the amide spins located at the crystallite surface from those located in the crystallite interior.[4] Note that the 70/30 separation of the spin–lattice magnetization into two components for both deuterated rings is similar to the 75/25 discrimination of populations for the amide sites of the N–D-labeled polymer.[5]

The identification of two populations in the spin–lattice relaxation data is not reflected in the T_1 discriminated line shape data for either PPD/T(d$_4$) or PPD(d$_4$)/T. From

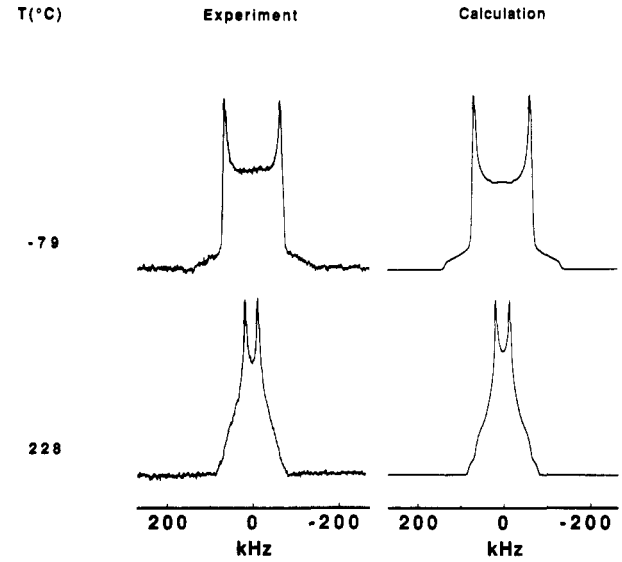

Figure 2. ^{2}H NMR experimental and calculated line shapes using a π-flip model (e^2qQ/h = 180 kHz) for poly(*p*-phenyleneterephthalamide) [PPD(d_4)]. The calculated line shape for −79 °C has a correlation time of 1.0 s and Gaussian broadening of 3.0 kHz. The calculated line shape for 228 °C has a correlation time of 1.0×10^{-9} s, a Gaussian broadening of 1.0 kHz, and a bimodal librational amplitude distribution.

a cursory line shape analysis in the low-temperature range, the fraction of rapid π-flippers for PPD/T(d_4) varies from nearly 0% at −79 °C to 25% near 50 °C, yet over this temperature range the line shapes associated with the two T_1 components both contain contributions from π-flipping and nonflipping components. The PPD(d_4)/T experimental line shapes show relatively little variation from a rigid, Pake-like spectrum over the range of −79 to 0 °C. For this site, the two spin–lattice relaxation times differ by at least a factor of 20 and magnetization can be selectively generated for the more mobile (crystallite surface) domain by using a delay (τ_0) in the saturation recovery sequence equal to 5 times the value of the smaller spin–lattice relaxation time (T_{1short}). This T_1 discrimination experiment results in similar line shapes for both T_{1short} and T_{1long} components. At all accessible temperatures, the line shapes are similar because both the fast-relaxing and the slow-relaxing components are in the slow to intermediate exchange regime for the processes reflected in the line shapes. The process which produces the line shape quadrupolar refocusing time (τ_1) dependence in PPD(d_4)/T is a π-flipping motion whose mean correlation time is less than 10^{-7} s (fast exchange) only when the temperature is above 139 °C (see Figure 2); this process is not fast enough to produce T_1 discrimination. The spin–lattice relaxation time discrimination data reflect a population associated with restricted angle rapid motion near the Larmor frequency (3×10^7 Hz) and is not related to the π-flip process. This mode of motion, which permits the T_{1short} component to be isolated, differentiates the population of spins at the crystallite surface or near defect regions from the majority population. Therefore, the dynamic structure is partially characterized as consisting of two populations whose spin–lattice relaxation times differ as a result of crystalline morphology.

Slow Exchange and Fast Exchange Line Shapes. The spin–lattice relaxation behavior indicates that at one level the dynamic structure is characterized by two populations of diamine rings with differing mobilities reflecting different crystalline environments. However, the line shape data indicate that each population also exhibits a distribution of π-flipping rates. In order to develop a motional model for the dynamics of the diamine rings, a simplified model was adopted. This approach was required because of the large number of variables required to fully model the line shape behavior. Specifically, the two populations (I and II) which may be temperature dependent are associated with a semirigid (constrained) component and a mobile (free) component. Each population has its own librational amplitude distribution $P(\Delta\theta)$, correlation time distribution $P(\tau_c)$, and a Gaussian broadening which is temperature dependent due to dipolar averaging. To determine suitable values for some of these variables, the slow exchange (low-temperature) and fast exchange (high-temperature) line shapes were simulated with a motional model with a minimum number of model parameters. The best values of these parameters, such as Gaussian broadening, were estimated from these calculations and incorporated into a basis set of line shapes to test a simplified motional model for the intermediate temperature range (6–118 °C).

For PPD(d_4)/T, Figure 2 illustrates the ^{2}H NMR experimental and calculated line shapes (e^2qQ/h = 180 kHz) for the lowest and highest temperature line shapes to be fit with the model. Over a temperature range of −79 to 0 °C, the fully-relaxed ^{2}H NMR experimental line shape appears as essentially a rigid, Pake-like powder pattern with very little delay time (τ_1) dependence. The calculated line shape is assumed to be in the slow motion limit and incorporates no librational motion. A visual fit to the experimental line shape (−79 °C) was accomplished by using a Gaussian broadening of 3 kHz to account for any librational motion, dipolar interaction, or dynamic heterogeneity present in the experimental line shape.

Figure 2 also illustrates the ^{2}H NMR experimental (228 °C) and calculated line shapes using a π-flip model (e^2qQ/h = 180 kHz). Over a temperature range of 139–228 °C, the experimental line shape did not vary and essentially no τ_1 dependence was observed. The line shape calculation was performed in the fast motion limit for *all* modes of motion with an arbitrarily chosen τ_c of 1.0×10^{-9} s for π-flips and a bimodal librational amplitude distribution ($P(\Delta\theta)$). The width of the line shape singularities were reproduced with a Gaussian broadening of 1 kHz to account for residual dipolar interactions.

In contrast to previous studies of the terephthalamide ring dynamics,[3] the high-temperature experimental line shape (228 °C; Figure 2) for the diamine rings could not be fit using an inhomogeneous Gaussian librational amplitude distribution $P(\Delta\theta)$ of standard deviation $\Delta(\Delta\theta)$ truncated at $\Delta\theta_0$ with $P(\Delta\theta) = 0$ for $\Delta\theta < \Delta\theta_0$. In particular, the zero frequency intensity could not be simulated unless a bimodal librational amplitude distribution was employed. Calculations of fast exchange π-flip line shapes for individual librational amplitudes indicated that the observed line shape intensity near zero frequency could be attributed to librational amplitudes near 40°. The bimodal librational amplitude distribution's exact shape could not be uniquely determined; however, previous experience from studies of the dynamics of the amide sites and the terephthalamide rings suggested a 75/25 bimodal librational amplitude distribution with the minor component associated with a larger amplitude of librational motion for the rapidly π-flipping rings. This librational distribution is shown in Figure 3 and was constructed from two Gaussian distributions. The major component (75%) has a low-angle cutoff of 4°, peak amplitude of 8°, standard deviation of 6°, and a mean librational amplitude of 10°, and the minor component (25%) has a low-angle cutoff of 20°, peak amplitude of 40°, standard deviation of 4°,

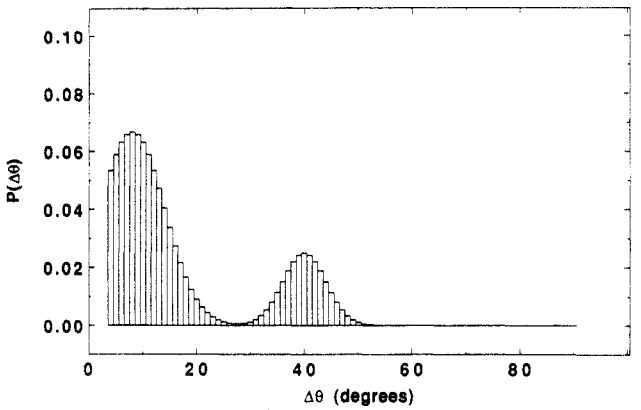

Figure 3. Librational amplitude distribution for rapidly π-flipping phenyl rings of poly(*p*-phenyleneterephthalamide) [PPD-(d_4)]. The distribution is composed of two Gaussian distributions. The major component (75%) has a low-angle cutoff of 4°, peak amplitude of 8°, and standard deviation of 6°. The minor component (25%) has a low-angle cutoff of 20°, peak amplitude of 40°, and standard deviation of 4°.

and a mean librational amplitude of 40°. Consistent with the discrimination of the amide site dynamics, the larger librational amplitude (near 40°) is associated with a more mobile component and may correspond to incomplete hydrogen-bonding near the crystallite surface or in defect regions.

The singularities and major features of the high and intermediate temperature experimental line shapes indicated that the motion of the diamine rings could be approximately described as a π-flip with additional rapid libration about the 1,4-diamine ring axis. Attenuation of residual dipolar interactions as temperature increased was indicated by the width of the singularities in the high temperature line shape which could be reproduced with a Gaussian broadening of only 1 kHz. A small decrease in the splitting between the experimental line shape singularities was observed as temperature increased. This could be due to a fairly narrow distribution of flipping angles about an exact π-flip. The sensitivity of the separation between the line shape singularities to the standard deviation of a Gaussian distribution of flip angles about an exact π-flip is illustrated in Figure 4. The experimentally observed decrease in splitting indicates that the standard deviation of a Gaussian distribution of flip angles centered about an exact π-flip would be less than 10°. Since this small variation from an exact π-flip results in a minor change in the line shape, a distribution of flipping angles about an exact π-flip was excluded from the simplified model which was used to simulate the intermediate temperature (6–118 °C) line shapes.

Intermediate Exchange Line Shapes: Simplified Model. A complete line shape analysis would take into account the two populations, possible temperature dependence of the populations, amplitude distributions for the rapid librational motions for each population ($P_I(\Delta\theta)$ and $P_{II}(\Delta\theta)$), correlation time distributions for each population ($P_I(\tau_c)$ and $P_{II}(\tau_c)$), and Gaussian broadening for each population. Each librational amplitude distribution and correlation time distribution requires a minimum of two variables (variance and mean). Thus there are at least 12 model variables. The analysis becomes tractable by reducing this number of model variables to 2. This is done by adopting *a simplified model which uses one population, uses one Gaussian broadening to account for dipolar interactions, ignores any libration, and considers only a symmetric log–Gaussian distribution of correlation times with the mean correlation time and the standard deviation as the only variables.* Hence, a basis set was generated for calculation of line shapes in the intermediate temperature range (6–118 °C) consisting of a slow exchange, Pake-like line shape [$\tau_c > 10^{-2}$ s, no libration, Gaussian broadening of 3 kHz (discussed above)]; an intermediate exchange set of π-flip line shapes [10^{-2} s $\geq \tau_c \geq 10^{-7}$ s, no libration, Gaussian broadening of 1 kHz]; and a fast exchange, π-flip lineshape (discussed above) [$\tau_c < 10^{-7}$ s, 75/25 bimodal librational amplitude distribution (discussed above), Gaussian broadening of 1 kHz]. Figure 5 shows the fully-relaxed ^{2}H NMR experimental and calculated line shapes for PPD(d_4)/T at a temperature of

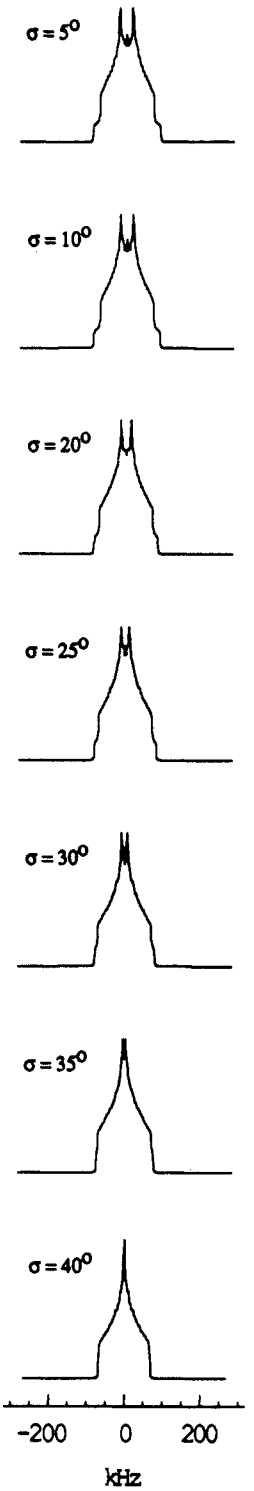

Figure 4. ^{2}H NMR calculated line shapes (e^2qQ/h = 180 kHz) for a Gaussian distribution (standard deviation σ) of flip angles centered about an exact π-flip. Line shapes are calculated in the fast motion limit for the π-flip motion.

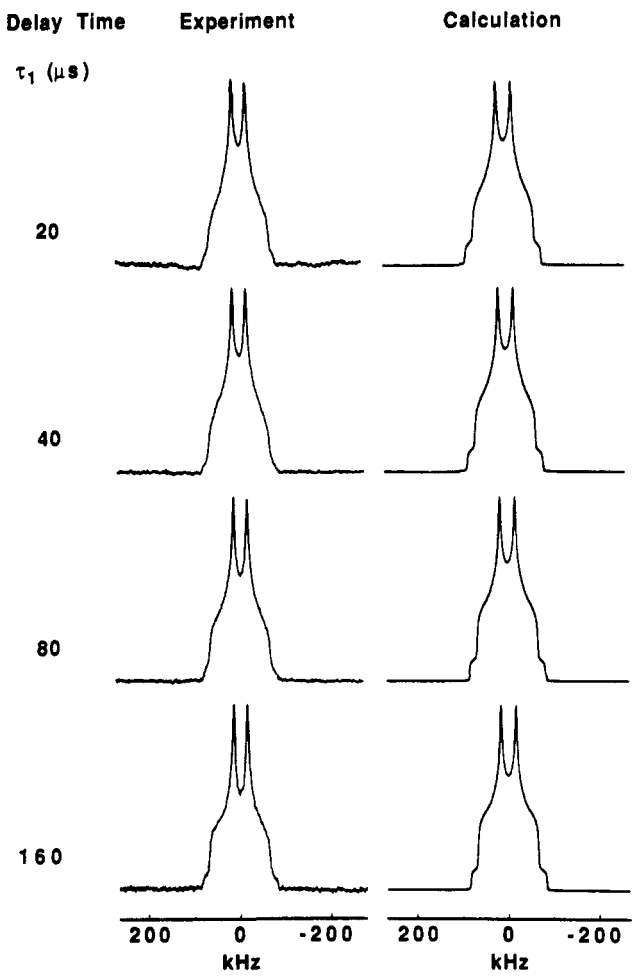

Figure 5. ^{2}H NMR experimental (118 °C) and calculated line shapes using a π-flip model (e^2qQ/h = 180 kHz) for poly(p-phenyleneterephthalamide) [PPD(d_4)]. Calculated line shapes are for an inhomogeneous log–Gaussian distribution of correlation times with σ = 1.0 decade centered at 2.5 × 10^{-7} s.

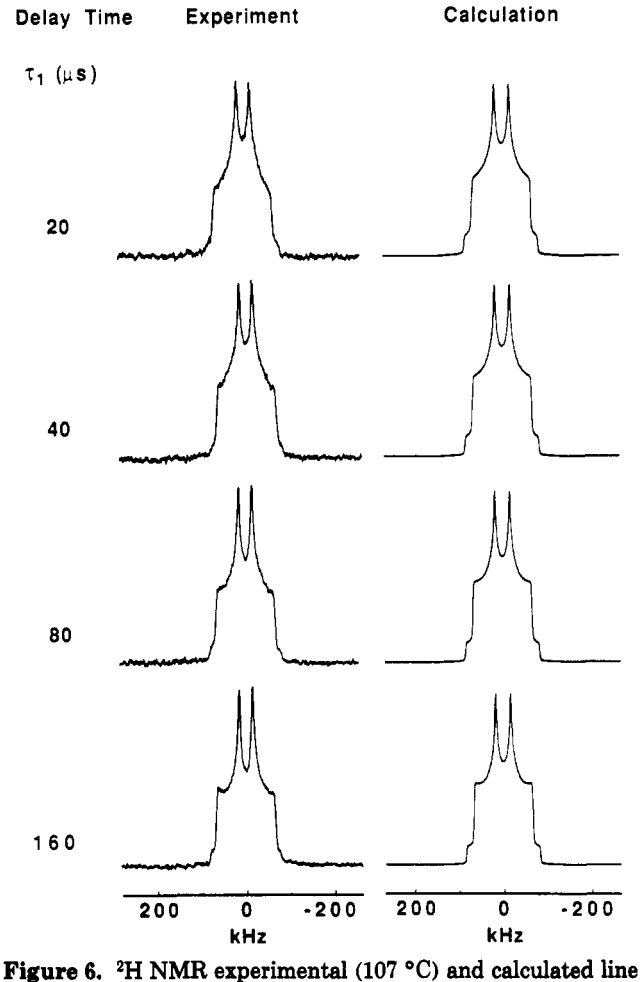

Figure 6. ^{2}H NMR experimental (107 °C) and calculated line shapes using a π-flip model (e^2qQ/h = 180 kHz) for poly(p-phenyleneterephthalamide) [PPD(d_4)]. Calculated line shapes are for an inhomogeneous log–Gaussian distribution of correlation times with σ = 1.5 decades centered at 1.6 × 10^{-6} s.

118 °C with delay times of 20, 40, 80, and 160 μs in the quadrupole echo pulse sequence. The calculated line shapes were produced using the simplified π-flip model with an inhomogenous symmetric log–Gaussian distribution of correlation times of standard deviation σ = 1.0 decade centered at 2.5 × 10^{-7} s. The experimental and calculated line shapes in Figure 5 are in reasonable agreement, except for differences near the outer edges of the line shapes; these differences could have been accounted for by restricted angle fluctuations, but are excluded (except in the fast exchange regime) from the simplified model. Additionally, the observed reduced line shape intensity near zero frequency is not fully accounted for in the calculated line shape at the longest delay time. This is indicative of the onset of yet another motional process outside of the scope of this model.

Figure 6 shows the fully-relaxed experimental (107 °C) and calculated line shapes. The calculated line shapes were produced using the simplified π-flip model with an inhomogenous log–Gaussian distribution of correlation times of standard deviation σ = 1.5 decades centered at 1.6 × 10^{-6} s. The calculated line shapes agree quite well with the experimental line shapes considering the caveats discussed for Figure 5. In comparison to the spectra at 118 °C, the increased intensity at the edges of the experimental line shape at 107 °C indicates the presence of a larger fraction of sites with longer correlation times, and this is reflected by the larger standard deviation and longer mean correlation time of the calculated line shape.

Figures 7 and 8 show the fully-relaxed experimental and calculated line shapes at 97 and 75 °C. Both sets of calculated line shapes use σ = 1.5 decades with a mean τ_c of 4.0 × 10^{-6} or 1.6 × 10^{-5} s, respectively. Calculated and experimental line shapes are in good agreement and the longer correlation time component, which produces the outer singularities in the line shape, becomes more prominent.

At 51 °C (Figure 9), the calculated line shapes again use σ = 1.5 decades, but now the correlation time distribution is centered at 2.5 × 10^{-5} s. The τ_1 dependence of the experimental and calculated line shapes are not in good agreement at long delay times where the experimental line shapes show a more pronounced intensity reduction near the middle of the line shape. This observation is in agreement with the spin–lattice relaxation results which indicate that the process (small angle fluctuations) which causes T_1 discrimination will begin to have a significant component of its spectral density function near 10^7 Hz for the larger population at this temperature and this process will result in a diminution of the center of the line shape.[16]

The ^{2}H NMR experimental line shapes for PPD(d_4)/T at 23 °C are shown in Figure 10, and these are similar to those observed at 6 °C, which are not shown. The calculated line shapes use σ = 1.5 decades with a mean correlation time centered at 6.3 × 10^{-5} s. Minor differences in the outer edge of the line shape near the baseline are, again, due to librational motion which was excluded from the model. The relatively poor fit near the center of the line shape could be substantially improved by invoking a

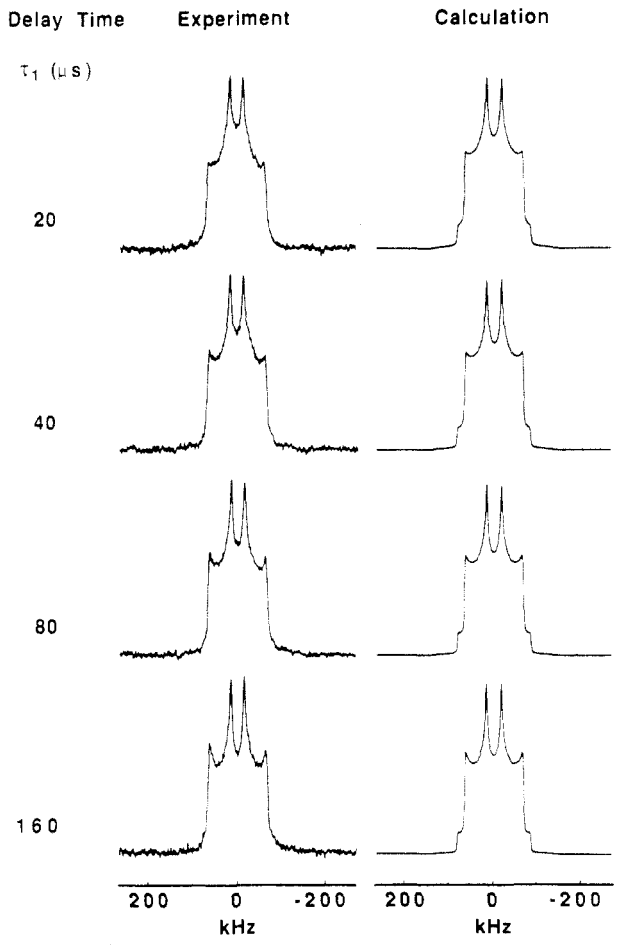

Figure 7. ^{2}H NMR experimental (97 °C) and calculated line shapes using a π-flip model (e^2qQ/h = 180 kHz) for poly(*p*-phenyleneterephthalamide) [PPD(d_4)]. Calculated line shapes are for an inhomogeneous log–Gaussian distribution of correlation times with σ = 1.5 decades centered at 4.0 × 10^{-6} s.

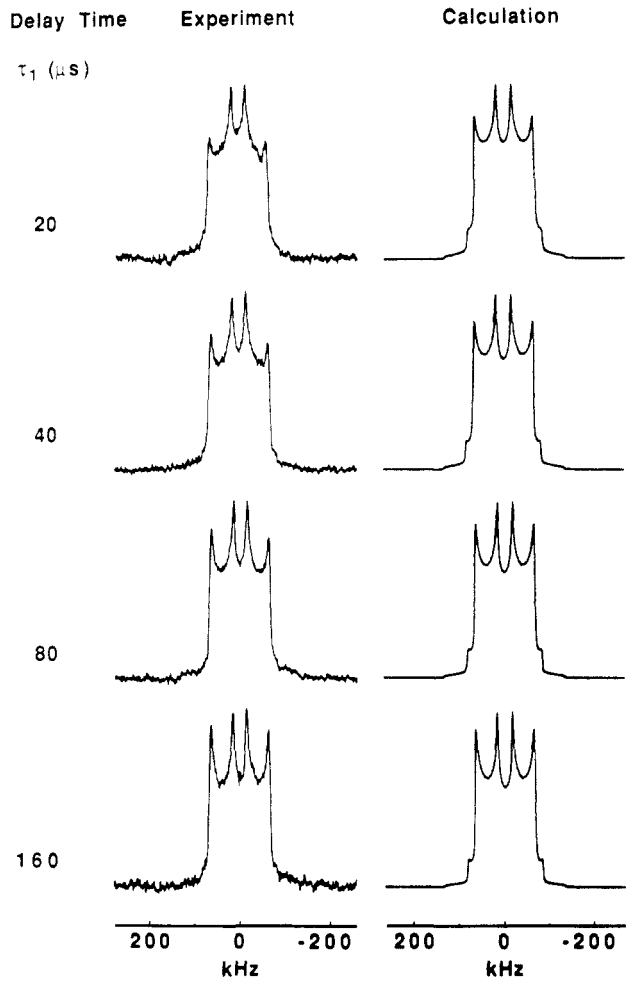

Figure 8. ^{2}H NMR experimental (75 °C) and calculated line shapes using a π-flip model (e^2qQ/h = 180 kHz) for poly(*p*-phenyleneterephthalamide) [PPD(d_4)]. Calculated line shapes are for an inhomogeneous log–Gaussian distribution of correlation times with σ = 1.5 decades centered at 1.6 × 10^{-5} s.

small-angle fluctuation, as was discussed for the 51 °C line shapes, along with a broader distribution of correlation times for π-flipping.

Over a temperature range of 6–118 °C, line shapes calculated from the simplified π-flip model are in reasonable agreement with the experimental line shapes, given the limitations of the model. This conclusion is further supported by the fairly good agreement of the calculated and experimental integrated magnetization reduction factors (Table I) corresponding to the line shapes in Figures 5–10. After correction of the experimental reduction factors to account for T_2(dipolar) interactions (which are partially averaged at higher temperatures), the agreement between experiment and calculation indicates that the major motional processes responsible for the experimentally observed line shapes are reasonably well described by the model.

Using the mean correlation time determined from the calculated line shapes for PPD(d_4)/T at temperatures of 23–118 °C, Figure 11 shows a plot of the logarithm of the inverse mean correlation time as a function of inverse temperature. A least squares fit of all of this data for the diamine rings resulted in an activation energy of 12 kcal/mol, which is comparable with the mean activation energy determined in a previous line shape analysis of the terephthalamide ring dynamics.[2] This activation energy has no physical meaning in either case, as it ignores the heterogeneity of the crystals. Fitted lines in the plot are intended to represent the separation of the data into two temperature regimes. The values of activation energies for each fitted line, 5 kcal/mol for the low-temperature data and 40 kcal/mol for the high-temperature data, illustrate the substantial dynamic difference between the two temperature regimes. This behavior is not due to an Arrhenius or WLF process but originates from two populations where the low-temperature regime is dominated by the dynamics of the crystallite surface (or defect regions) and the high-temperature regime is dominated by the dynamics of the crystallite interior.

The separation of PPTA dynamics into two motional regimes can also be found by examination of the line shape analysis for the terephthalamide rings (PPD/T(d_4)) previously studied with a bimodal correlation time model.[3] Figure 12 shows the logarithm of the fraction (P_f) of rapidly π-flipping terephthalamide rings as a function of inverse temperature. The plotted lines visually indicate the separation of the dynamics of the terephthalamide rings into two motional regimes separated by a transition temperature regime. Slopes of the plotted lines are similar with an apparent "activation energy" near 1.3 kcal/mol. At the transition region, the fraction of π-flippers is near 25% and the fraction of nonflippers is near 75%. The 75/25 population distribution is similar to the 70/30 population distribution observed in the spin–lattice relaxation amplitudes of the diamine and terephthalamide rings and the amide site 75/25 population distribution. The similar population distributions observed for the diamine rings, terephthalamide rings, and amide sites are consistent with a more mobile minor population being associated with the crystallite surface (or defect regions)

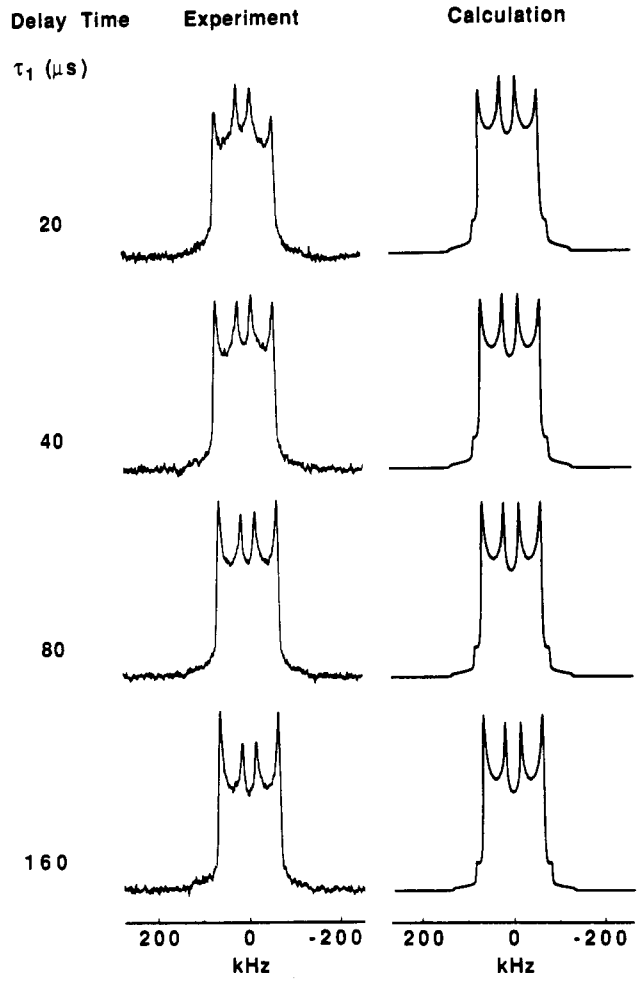

Figure 9. ^{2}H NMR experimental (51 °C) and calculated line shapes using a π-flip model (e^2qQ/h = 180 kHz) for poly(*p*-phenyleneterephthalamide) [PPD(d_4)]. Calculated line shapes are for an inhomogeneous log–Gaussian distribution of correlation times with σ = 1.5 decades centered at 2.5 × 10^{-5} s.

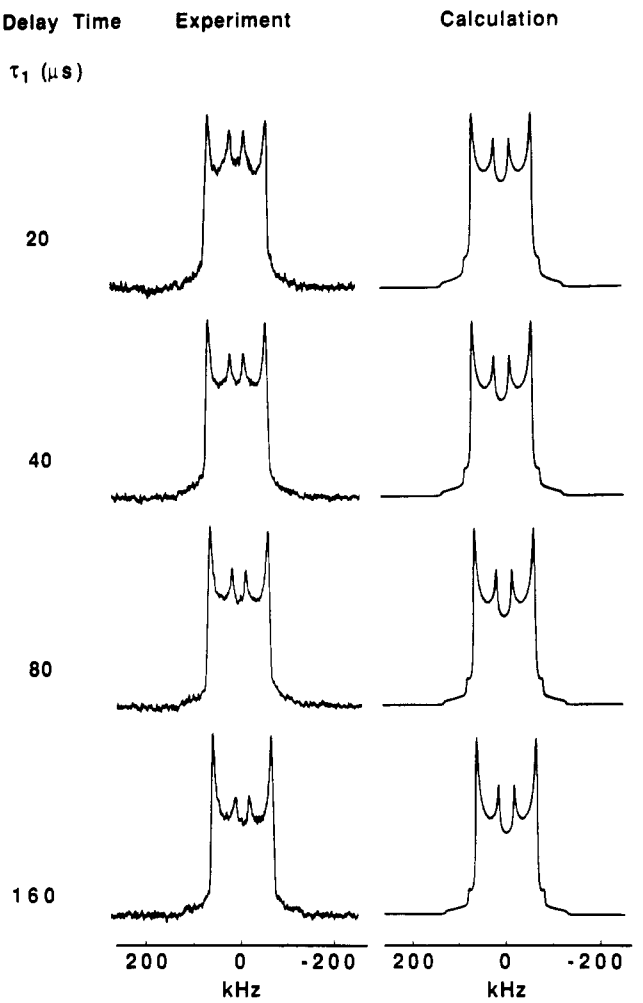

Figure 10. ^{2}H NMR experimental (23 °C) and calculated line shapes using a π-flip model (e^2qQ/h = 180 kHz) for poly(*p*-phenyleneterephthalamide) [PPD(d_4)]. Calculated line shapes are for an inhomogeneous log–Gaussian distribution of correlation times with σ = 1.5 decades centered at 6.3 × 10^{-5} s.

and the relatively less mobile majority population being associated with the crystallite interior.[5]

Dynamic Structure Summary

The current results taken in concert with previous[1,2,4] and concurrent results[3,5] yield a description of the dynamic structure of PPTA at the segmental level. The observations that have led to this description and the resulting conclusions are summarized here.

First, the magnetization for the selectively deuterated diamine rings and terephthalamide rings may be effectively separated by spin–lattice relaxation time discrimination into a relatively rigid "constrained" component and a relatively mobile "free" component. Furthermore, the present results indicate that the process responsible for this discrimination is not a π-flip (large-angle jump) of the diamine or terephthalamide ring, but likely is a restricted angle fluctuation (rapid librational motion) that occurs with a rate near the Larmor frequency.

Second, the key to understanding the dynamic structure is provided by the amide N–D motion.[4,5] The line shapes for the N–D bonds could be decomposed into a major component (75%) associated with a "constrained" population and a minor component (25%) associated with a "free" population executing a large-angle jump. This behavior is temperature-independent, and the "free" population has been associated[5] with the crystallite surface which is incompletely hydrogen-bonded.

Table I. Integrated Magnetization Reduction Factors

T (°C)	τ_1 (μs)	expt[a,b,c]	calc[a]
23[d]	40	0.90	0.82
	80	0.75	0.65
	160	0.71	0.50
51	40	0.84	0.83
	80	0.71	0.66
	160	0.54	0.53
75	40	0.86	0.83
	80	0.66	0.67
	160	0.61	0.53
97	40	0.84	0.85
	80	0.69	0.72
	160	0.63	0.60
107	40	0.81	0.87
	80	0.70	0.76
	160	0.69	0.66
118	40	0.98	0.93
	80	0.86	0.85
	160	0.79	0.76

[a] All data normalized to the value of magnetization at τ_1 = 20 μs. [b] Experimental data corrected for T_2(dipolar) where the average magnetization reduction due to this factor over the temperature range −80 to −15 °C is 0.91 (40 μs), 0.77 (80 μs), and 0.48 (160 μs). [c] Experimental values over the temperature range 140–230 °C are equal to 1.0 after modification to account for T_2(dipolar). [d] Data for 6 °C is similar to data for 23 °C.

Third, the present results indicate that the "constrained" and "free" populations, associated with the crystallite interior and surface, respectively, are heterogeneous. The

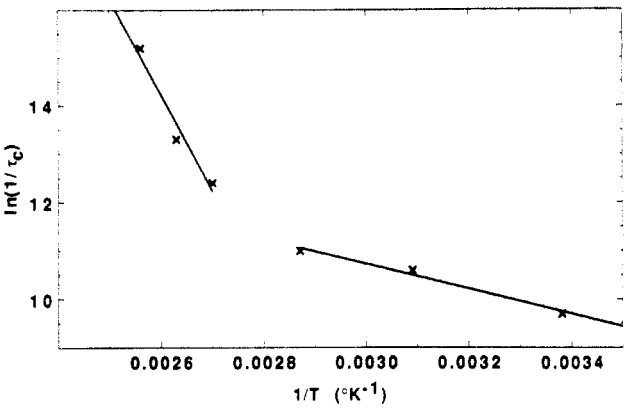

Figure 11. Logarithm of the inverse mean correlation time of an inhomogeneous log–Gaussian distribution of correlation times vs inverse temperature for poly(*p*-phenyleneterephthalamide) [PPD(d_4)].

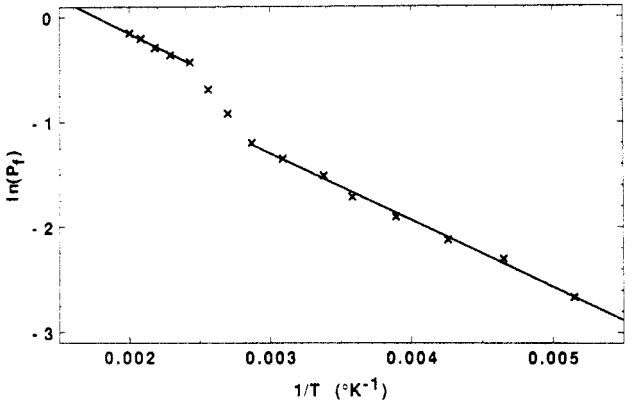

Figure 12. Logarithm of the fraction (P_f) of rapidly π-flipping terephthalamide rings vs inverse temperature for poly(*p*-phenyleneterephthalamide) [T(d_4)]. Data from bimodal correlation time model.

non-hydrogen-bonded surface sites are dynamically heterogeneous in that the fraction of rings (both terephthalamide and diamine) that are able to execute a π-flip is temperature-dependent. This indicates that the surface sites, that are effectively differentiated by more rapid spin–lattice relaxation, have a distribution of jump rates or enabling free volume and hence are heterogeneous with respect to the ability to execute a π-flip. Substantial heterogeneity within the crystallites is likewise indicated by the very large temperature range necessary to enable all terephthalamide rings to flip and the direct observation of a distribution of jumping rates for the diamine rings. For the diamine rings, the observation that the activation energies associated with the π-flipping process vary by nearly 1 order of magnitude for the two populations (free and constrained) demonstrates that there are two populations of rings with very different environments; furthermore, the distribution of correlation times determined at each temperature demonstrates that both populations are heterogeneous.

Lastly, this description of the dynamic structure is consistent with a recent description of the morphology of PPTA developed[5] from X-ray diffraction, TEM, amide accessibility to heavy water exchange, and Raman and NMR spectroscopies. This description characterizes the structure as having either relatively small crystallites orthogonal to the chain axis direction or, alternatively,[5] planes containing a large concentration of structural defects. The dynamic structure expands this description to identify that both the crystal surfaces (or defect planes) and the crystallite interiors (or more perfectly aligned planes) are dynamically heterogeneous from the perspective of terephthalamide or diamine ring π-flips. Thus the dynamic structure of PPTA at the segmental level further illustrates the complex nature of the intra- and intermolecular structure of this polymer on a length scale from 1 to 100 Å.

Acknowledgment. We are indebted to P. A. Cooper for skilled technical assistance.

References and Notes

(1) Cain, E. J.; Gardner, K. H.; Gabara, V.; Allen, S. R.; English, A. D. *Polym. Prepr. (Am. Chem. Soc., Div. Polym. Chem.)* **1990**, *31*, 518.
(2) Cain, E. J.; Gardner, K. H.; Gabara, V.; Allen, S. R.; English, A. D. *Macromolecules* **1991**, *24*, 3721.
(3) Schadt, R. J.; Cain, E. J.; Gardner, K. H.; Gabara, V.; Allen, S. R.; English, A. D. *Macromolecules*, previous paper in this issue.
(4) Schadt, R. J.; Cain, E. J.; Gardner, K. H.; Gabara, V.; Allen, S. R.; English, A. D. *Polym. Prepr. (Am. Chem. Soc., Div. Polym. Chem.)* **1991**, *32*, 253.
(5) Jackson, C. L.; Schadt, R. J.; Gardner, K. H.; Chase, D. B.; Allen, S. R.; Gabara, V.; English, A. D. *Polymer*, in press.
(6) English, A. D.; Gardner, K. H.; Schadt, R. J.; Cain, E. J.; Gabara, V.; Allen, S. R. *Polym. Prepr. (Am. Chem. Soc., Div. Polym. Chem.)* **1992**, *33*, 82.
(7) Northolt, M. G. *Eur. Polym. J.* **1974**, *10*, 799.
(8) Haraguchi, K.; Kajiyama, T.; Takayanagi, M. *J. Appl. Polym. Sci.* **1979**, *23*, 915.
(9) Panar, M.; Avakian, P.; Blume, R. C.; Gardner, K. H.; Gierke, T. D.; Yang, H. H. *J. Polym. Sci. Polym. Phys. Ed.* **1983**, *21*, 1955.
(10) Tanner, D.; Fitzgerald, J. A.; Phillips, B. R. *Adv. Mater.* **1989**, *51*, 151.
(11) Chase, D. B. *Microchim. Acta* **1987**, *3*, 81.
(12) Gerstein, G. C. *Philos. Trans. R. Soc. London A* **1981**, *299*, 521.
(13) Hentschel, R.; Spiess, H. W. *J. Magn. Reson.* **1979**, *35*, 157.
(14) Henrichs, P. M.; Hewitt, J. M.; Linder, M. *J. Magn. Reson.* **1984**, *60*, 280.
(15) Ronemus, A. D.; Vold, R. L.; Vold, R. R. *J. Magn. Reson.* **1986**, *70*, 416.
(16) Hirschinger, J.; Miura, H.; Gardner, K. H.; English, A. D. *Macromolecules* **1990**, *23*, 2153.
(17) Bloom, M.; Davis, J. H.; Valic, M. I. *Can. J. Phys.* **1980**, *58*, 1510.
(18) Spiess, H. W.; Sillescu, H. *J. Magn. Reson.* **1981**, *42*, 381.
(19) Barbara, T. M.; Greenfield, M. S.; Vold, R. L.; Vold, R. R. *J. Magn. Reson.* **1986**, *69*, 311.
(20) Schadt, R. J.; English, A. D. *J. Phys. Chem.* **1993**, *97*, 8387.